

Multi-scale theories for the MJO

Andrew J. Majda and Samuel N. Stechmann

November 24, 2010

1 Introduction

In the equatorial troposphere, the Madden–Julian Oscillation (MJO) is a planetary-scale wave envelope of complex multi-scale convection (see Figure 1 for a schematic illustration). It begins as a standing wave in the Indian Ocean and propagates eastward across the western Pacific Ocean at a speed of ≈ 5 m/s. Due to its planetary-scale circulation anomalies, the MJO significantly affects monsoon development, intraseasonal predictability in midlatitudes, and the development of the El Niño southern oscillation (ENSO) in the Pacific Ocean, which is one of the most important components of seasonal prediction (Zhang, 2005; Lau and Waliser, 2005). It is also known that the MJO is a superrotating planetary-scale wave [see Biello et al. (2007) and references therein], and recent simulations suggest there may be enhanced MJO activity in a warmer climate, possibly leading to a superrotating tropical mean circulation (Caballero and Huber, 2010).

Basic understanding of the MJO’s features has been gained from observations, including statistical composites (Salby and Hendon, 1994; Hendon and Salby, 1994; Hendon and Liebmann, 1994; Wheeler and Kiladis, 1999; Roundy and Frank, 2004; Kiladis et al., 2005) and case studies of individual MJO events (Lin and Johnson, 1996; Yanai et al., 2000; Houze et al., 2000). From these observations, the following fundamental features of the MJO have been identified relatively clearly:

- I. slow eastward phase speed of ≈ 5 m/s,
- II. peculiar dispersion relation of $d\omega/dk \approx 0$,
- III. horizontal quadrupole vortex structure.

In the simplest theoretical model for the MJO, its vertical structure is given by the first baroclinic mode, and its horizontal structure is given by the planetary-scale response to a moving heat source whose velocity is prescribed at the MJO speed (Matsuno, 1966; Gill, 1980; Chao, 1987). This is called the Kelvin–Rossby wave paradigm by Houze et al. (2000), and they use it as a rough guideline for understanding observations, even though the structure of the model is different from and often at odds with the actual observations (Houze et al., 2000). In fact, many theories have been proposed for the MJO, but they are

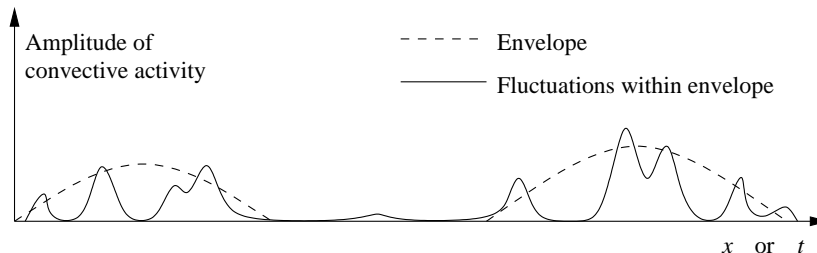


Figure 1: A large-scale envelope with fluctuations embedded within it.

all at odds with the observations in various crucial ways, and no theory for the MJO has yet been generally accepted [see Majda and Stechmann (2009a) and Wang (2005) for overviews]. The present subchapter describes several recent theories and models for the MJO which focus on the multi-scale structure of the MJO envelope (as described schematically in Figure 1).

This subchapter begins with a minimal dynamical model for the MJO skeleton which captures all of the three key features I–III listed above. The following section deals with details of the MJO structure beyond the fundamental features of the skeleton, such as the vertical structure and the impact of multi-cloud and multi-scale effects. Then we discuss the implications of these theories for improving global circulation model (GCM) simulations of the MJO.

2 The MJO Skeleton

The MJO skeleton model is a minimal dynamical model that recovers robustly all three of the fundamental features I–III listed above. The fundamental mechanism of this model was proposed and developed in Majda and Stechmann (2009a), and it involves neutrally stable interactions between (i) planetary-scale, lower-tropospheric moisture anomalies and (ii) synoptic-scale, convectively-coupled-wave activity (or, more precisely, the planetary-scale envelope of this synoptic-scale convective activity).

The behavior of these two phenomena, the moisture and wave activity, has been documented in numerous previous studies. Several studies have shown that the lower troposphere tends to moisten during the suppressed-convection phase of the MJO, and lower-tropospheric moisture appears roughly in quadrature with the MJO’s heating anomaly (Kikuchi and Takayabu, 2004; Kiladis et al., 2005; Tian et al., 2006). Furthermore, it is well-known that the low-level moisture content plays a key role in regulating mesoscale convection, and there is growing evidence that it also plays a key role in regulating convection on the scales of synoptic-scale convectively coupled waves and the MJO (Kikuchi and Takayabu, 2004; Kiladis et al., 2005; Khouider and Majda, 2006; Tian et al., 2006; Khouider and Majda, 2007; Majda et al., 2007; Khouider and Majda, 2008a). A fundamental part of the model presented in Majda and Stechmann

(2009a) is the effect of this low-level moisture on the envelope of synoptic-scale wave activity.

The important role of synoptic-scale wave activity in driving the MJO is documented in a growing body of evidence in the form of observations (Hendon and Liebmann, 1994; Houze et al., 2000; Masunaga et al., 2006), simulations (Grabowski, 2001, 2003; Grabowski and Moncrieff, 2004; Khouider and Majda, 2007; Majda et al., 2007; Majda and Stechmann, 2009b), and theory (Moncrieff, 2004; Majda and Biello, 2004; Biello and Majda, 2005, 2006; Biello et al., 2007). This synoptic-scale wave activity is a complex menagerie of convectively coupled equatorial waves, such as two-day waves, convectively coupled Kelvin waves, etc. (Khouider and Majda, 2006, 2008a; Kiladis et al., 2009), and the envelope of this wave activity drives the MJO with its convective heating anomalies (Biello and Majda, 2005).

Based on the mechanisms outlined above, a dynamic model is designed for the MJO skeleton on intraseasonal/planetary scales. The model is formulated in terms of anomalies from a uniform base state of radiative–convective equilibrium, $\bar{R} = \bar{H}\bar{a}$, where $\bar{R} = 1$ K/d is the fixed, constant radiative cooling rate, \bar{H} is a constant heating rate prefactor, and \bar{a} is a constant (nondimensional) amplitude of wave activity in the equilibrium state. The dry dynamical core of the model is the equatorial long-wave equations (Majda, 2003; Majda and Biello, 2004; Biello and Majda, 2005, 2006), and two other dynamic variables are included to represent moist convective processes: q , the lower tropospheric moisture; and a , the amplitude of the wave activity envelope. The nondimensional dynamical variable a parameterizes the amplitude of the planetary-scale envelope of synoptic-scale wave activity (see Figure 1). It is noteworthy that, for the MJO skeleton model discussed here and in Majda and Stechmann (2009a), it is only the amplitude of the wave activity envelope that is needed, not any of the details of the particular synoptic-scale waves (Khouider and Majda, 2006, 2008a; Kiladis et al., 2009) that make up the envelope. A key aspect of the model here is the interaction between a and q : as motivated by the discussion above, positive (negative) low-level moisture anomalies create a tendency to enhance (decrease) the envelope of equatorial synoptic-scale wave activity. The simplest equation for the wave activity with these features is $a_t = \Gamma q(\bar{a} + a)$. The wave activity envelope then feeds back on the other variables through a heat source $\bar{H}a$ and—in accordance with conservation of moist static energy—a moisture sink $-\bar{H}a$. Thus the model equations for the anomalies from radiative–convective equilibrium take the form

$$\begin{aligned}
 u_t - yv &= -p_x \\
 yu &= -p_y \\
 0 &= -p_z + \theta \\
 u_x + v_y + w_z &= 0 \\
 \theta_t + w &= \bar{H}a \\
 q_t - \tilde{Q}w &= -\bar{H}a \\
 a_t &= \Gamma q(\bar{a} + a).
 \end{aligned} \tag{1}$$

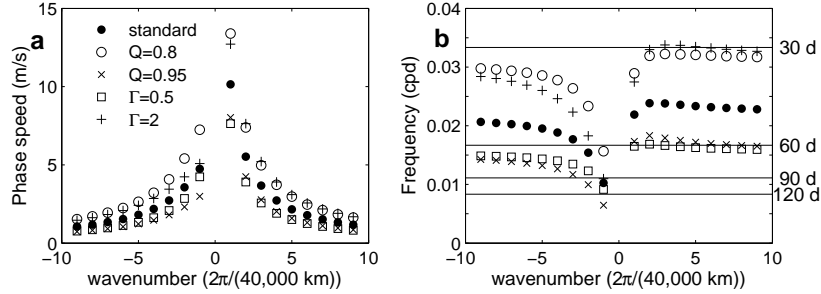


Figure 2: Phase speed (a) and oscillation frequency (b) as functions of wavenumber k for the low-frequency linear modes of the MJO skeleton model. Positive (negative) values of k represent eastward- (westward-) propagating modes. Different symbols represent different parameter choices. Adapted from Majda and Stechmann (2009a).

Here u , v , and w are the zonal, meridional, and vertical velocities, respectively; and p and θ are the pressure and potential temperature, respectively. Notice that this model contains a minimal number of parameters: $\tilde{Q} = 0.9$, the (nondimensional) mean background vertical moisture gradient; and $\Gamma = 1$, where Γq acts as a dynamic growth/decay rate of the wave activity envelope in response to moisture anomalies. In dimensional units, $\Gamma \approx 0.2 \text{ d}^{-1} \text{ K}^{-1}$. These will be the standard parameter values used here unless otherwise noted. Also notice that the parameter \bar{H} is actually irrelevant to the dynamics (as can be seen by rescaling (1) and recalling the equilibrium condition $\bar{R} = \bar{H}\bar{a}$), but it is written here for clarity of presentation.

The next step in obtaining the simplest dynamical model for the MJO skeleton is to use truncated vertical and meridional structures. The vertical structure is assumed to be first baroclinic [either $\cos(z)$ or $\sin(z)$] as in the Matsuno–Gill mean heating model (Majda, 2003; Biello and Majda, 2006). For instance, the zonal velocity u has a truncated vertical structure of $u(x, y, z, t) = \sum_j u_j(x, y, t)\sqrt{2}\cos(jz) \approx u_1(x, y, t)\sqrt{2}\cos z$. Truncated meridional structures are also used for simplicity. The meridional structure of a is assumed to simply be proportional to $\exp(-y^2/2)$. Such a meridional heating structure is known to excite only Kelvin waves and the first symmetric equatorial Rossby waves (Majda, 2003; Biello and Majda, 2006); hence one can write the resulting meridionally truncated equations as

$$\begin{aligned}
 K_t + K_x &= -\frac{1}{\sqrt{2}}\bar{H}A \\
 R_t - \frac{1}{3}R_x &= -\frac{2\sqrt{2}}{3}\bar{H}A \\
 Q_t + \frac{1}{\sqrt{2}}\tilde{Q}K_x - \frac{1}{6\sqrt{2}}\tilde{Q}R_x &= \left(-1 + \frac{1}{6}\tilde{Q}\right)\bar{H}A \\
 A_t &= \Gamma\bar{a}Q
 \end{aligned} \tag{2}$$

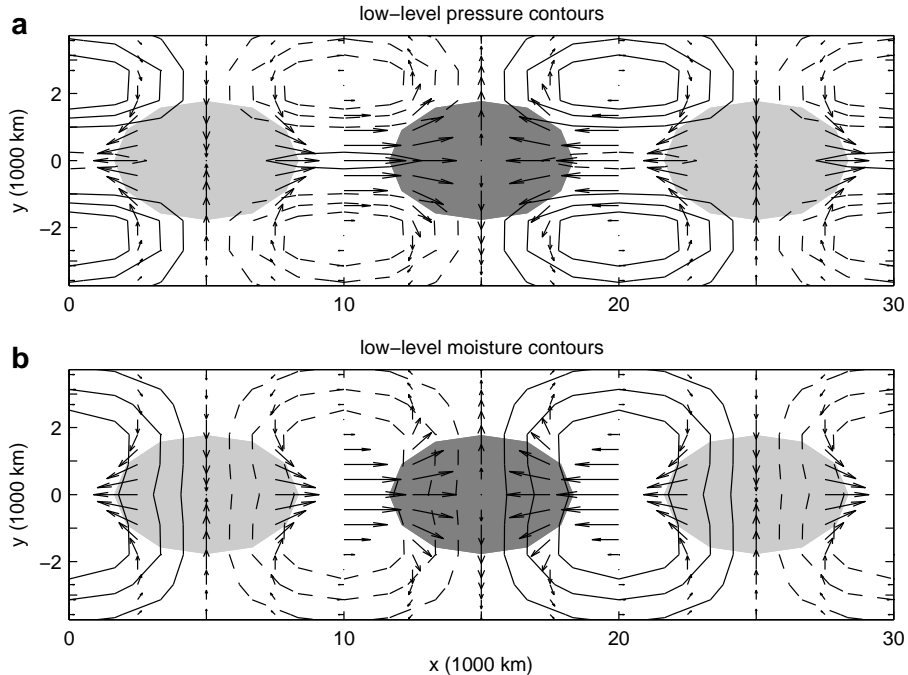


Figure 3: Horizontal structure of the wavenumber-2 MJO mode of the skeleton model. (a) Contours of lower-tropospheric pressure anomalies. (b) Contours of lower-tropospheric moisture anomalies. Solid (dashed) lines denote positive (negative) anomalies. Dark (light) shading denotes positive (negative) anomalies of convective activity. From Majda and Stechmann (2009a).

where K and R are the amplitudes of the Kelvin and equatorial Rossby waves, respectively, and they have the familiar meridional structures associated with them (Majda, 2003). In the absence of forcing, the “dry” long-wave Kelvin and equatorial Rossby wave solutions of (2) are dispersionless waves that propagate at 50 and 17 m/s, respectively (Majda, 2003; Biello and Majda, 2006). In the presence of the dynamical forcing A in (2), the Kelvin and equatorial Rossby waves can be coupled to each other and to Q and A , and these coupled modes can be dispersive.

Now the linear modes of the model are presented. Since the model (2) involves four dynamically coupled variables, there are four linear modes. The dispersion relation for the linear modes is shown in Figure 2. (Only the two low-frequency, intraseasonal modes are shown. The other two modes are high-frequency modes and are only weakly coupled to the wave activity.) Figure 2 shows that the skeleton model has eastward-propagating waves with phase speeds of roughly 5 m/s and the peculiar dispersion relation $d\omega/dk \approx 0$, in agreement with the MJO. Moreover, the phase speed and dispersion relation

are robust over a wide range of parameter values, with the oscillation periods spanning the range of 30–60 days, which is the observed range of the MJO’s oscillation period. The westward-propagating waves, on the other hand, which are plotted with positive ω and negative k , have variable ω , and their oscillation periods are seasonal, not intraseasonal, for $k = 1$ and 2 . This suggests the first piece of our explanation for the observed dominance of eastward-propagating intraseasonal variability: the westward-propagating modes have seasonal oscillation periods, on which time scales other phenomena are expected to dominate over modulations of synoptic-scale wave activity. The second piece of the explanation is that the eastward-propagating modes are more strongly coupled to equatorial moist convective processes than the westward-propagating modes (Majda and Stechmann, 2009a).

The physical structure of the wavenumber-2 MJO mode is shown in Figure 3 for the standard parameter values. Horizontal quadrupole vortices are prominent, as in observations, and the maximum wave activity is colocated with the maximum in equatorial convergence. The lower tropospheric moisture leads and is in quadrature with the wave activity, which is also roughly the relationship seen in observations (Kikuchi and Takayabu, 2004; Kiladis et al., 2005; Tian et al., 2006). The pressure contours clearly display the mixed Kelvin/Rossby wave structure of the wave. Equatorial high pressure anomalies are colocated with the westerly wind burst as in Kelvin waves; and they are flanked by off-equatorial low pressure anomalies and cyclonic Rossby gyres, in broad agreement with the observational record. Rectification of the vertical structure and some of the phase relationships is likely due to effects of higher vertical modes (Majda and Biello, 2004; Biello and Majda, 2005; Khouider and Majda, 2007; Majda et al., 2007), as discussed in the next section.

In addition to these illustrations, a formula for the intraseasonal oscillation frequency ω of the MJO skeleton can be obtained by considering the even simpler case of flow above the equator. In this case, v and y are set to zero, and meridional derivatives are ignored. The result is a linear system of four equations for u, θ, q, a , and the system can be solved exactly due to the perfect east–west symmetry:

$$2\omega^2 = \Gamma\bar{R} + k^2 \pm \sqrt{(\Gamma\bar{R} + k^2)^2 - 4\Gamma\bar{R}k^2(1 - \tilde{Q})} \quad (3)$$

where k is the zonal wavenumber. For the low-frequency waves, this is approximately equal to

$$\omega \approx \sqrt{\Gamma\bar{R}(1 - \tilde{Q})}, \quad (4)$$

For the standard parameter values used here, the oscillation period corresponding to (4) is 45 days, in agreement with observations of the MJO. Notice that this formula is independent of the wavenumber k ; i.e., this model recovers the peculiar dispersion relation $d\omega/dk \approx 0$ from the observational record, and it relates the MJO frequency to the three parameters of the model.

3 Multi-cloud and multi-scale effects

Beyond the fundamental features I–III explained by the MJO skeleton model, there are other observed details such as a refined vertical structure, a multi-cloud progression, and multi-scale convective processes. Regarding the refined vertical structure and multi-cloud effects, observations show a progression in the MJO through three cloud types above the boundary layer: in the initial phase, lower/middle-troposphere congestus cloud decks moisten and precondition the lower troposphere; then deep convection develops; and finally a trailing wake of upper-troposphere stratiform clouds follows (Lin and Johnson, 1996; Houze et al., 2000; Kikuchi and Takayabu, 2004; Kiladis et al., 2005). Concomitant with this progression in cloud types, the MJO envelope has a zonal–vertical tilt in heating, moisture, temperature, and circulation. For instance, in the initial phase, there is a low-level westerly onset region below easterlies; then strong westerlies develop in the deep convective region; and finally the strongest westerlies form aloft in the lower/middle troposphere in the stratiform region. Regarding multi-scale structure, observations also reveal complex multi-scale features within the propagating large-scale envelope of the MJO. These embedded smaller-scale features include westward-propagating two-day waves, eastward-propagating superclusters or convectively coupled Kelvin waves (Kiladis et al., 2009), and smaller-scale squall line clusters that typically propagate westward (Nakazawa, 1988; Houze et al., 2000).

To account for these refined features of the MJO, we next describe multi-cloud and multi-scale models and theories for them.

3.1 Kinematic models for the MJO

The multi-cloud aspects of the MJO are illustrated by a kinematic multi-scale model for the MJO (Majda and Klein, 2003; Majda and Biello, 2004; Biello and Majda, 2005; Biello et al., 2007), which generalizes the Matsuno–Gill heating models in two significant ways. First, rather than a first baroclinic mode structure, a general heating structure in the vertical is utilized; and second, upscale transport effects are modeled in a systematic multi-scale fashion, including upscale transports of momentum and temperature from the synoptic scales to the planetary scales. In Figure 4, we illustrate the vertical structure of the zonal winds along the equator for three cases of the model of Biello and Majda (2005), in order of increasing complexity and realism. Figure 4a shows results similar to the traditional Matsuno–Gill heating model; this case is different in that the mean heating includes both deep convection and stratiform contributions, but it is similar in that the updraft is upright (as opposed to the tilted updrafts below), which occurs because the deep convection and stratiform heating are colocated with each other in space/time. Figure 4b shows results from a congestus–deep–stratiform mean heating model, where the three contributions lag each other in space/time to create a tilted heating anomaly and a tilted updraft (Biello and Majda, 2005; Kiladis et al., 2005); note that the westerly wind burst begins at the bottom of the troposphere with easterly winds aloft

as in the observations (Lin and Johnson, 1996). Finally, in Figure 4c, besides the congestus–deep–stratiform mean heating, we also include the additional effects of upscale momentum transports (Majda and Biello, 2004). The upscale transports are derived from a plausible multi-cloud model of synoptic variability within the MJO envelope. As shown in Figure 4c, the strongest winds in the westerly wind burst now occur aloft in the lower–middle troposphere as the strong phase of the MJO proceeds; this is in qualitative agreement with observations (Lin and Johnson, 1996). Thus, Figure 4c captures all of the zonal and vertical qualitative aspects observed in the MJO; the model for Figure 4c also captures a number of observed features of the horizontal structure of the MJO (Biello and Majda, 2005; Biello et al., 2007).

An important aspect of the observational record for the MJO is that it is superrotating (Moncrieff, 2004); in other words, the large-scale, vertically averaged, zonal equatorial winds move faster than the planetary rotation. According to Hide’s Theorem, this observed superrotation implies that there necessarily must be upscale transports of momentum to sustain superrotation. Biello et al. (2007) use the multi-scale MJO models discussed here to show that the upscale fluxes from vertical transport of synoptic-scale momentum combined with positive planetary-scale heating drive this superrotation. In particular, there is no superrotation possible from planetary-scale heating alone in a Matsuno–Gill model; multi-scale effects are needed.

3.2 Dynamic models for waves in the MJO

Kinematic models for the MJO, like those in Figure 4, are highly simplified in that the MJO’s phase speed and heat source are specified. A more realistic approach should have an interactive heat source and should predict the MJO’s phase speed, as in the MJO skeleton model of section 1. An even more realistic approach should also resolve the smaller-scale fluctuations embedded within the MJO envelope, not just the planetary-scale envelope itself. The goal of this section is to review current understanding of the dynamic interactions between the MJO envelope and the fluctuations within the envelope. Since envelope–fluctuation interactions is a common, generic topic, we first review these interactions in different contexts, and then we review detailed results with application to the MJO specifically.

Envelope–fluctuation interactions are a common occurrence in the tropics, where the multi-scale hierarchy of organized convection can be divided into three broad categories: (i) the MJO on planetary spatial scales (roughly 20,000 km) and intraseasonal time scales (roughly 40 days) (Lau and Waliser, 2005; Zhang, 2005) (ii) convectively coupled waves (CCW) on equatorial synoptic scales (roughly 2,000 km and 4 days) (Kiladis et al., 2009), and (iii) mesoscale convective systems (MCS) on mesoscales (roughly 200 km and 0.4 days) (Houze, 2004). This hierarchy has a remarkable multi-scale structure: the MJO is an envelope of smaller-scale CCW, and, in turn, the CCW are envelopes of smaller-scale MCS. Figure 1 illustrates the structure of a generic large-scale envelope with smaller-scale fluctuations embedded within it. For such a multi-scale en-

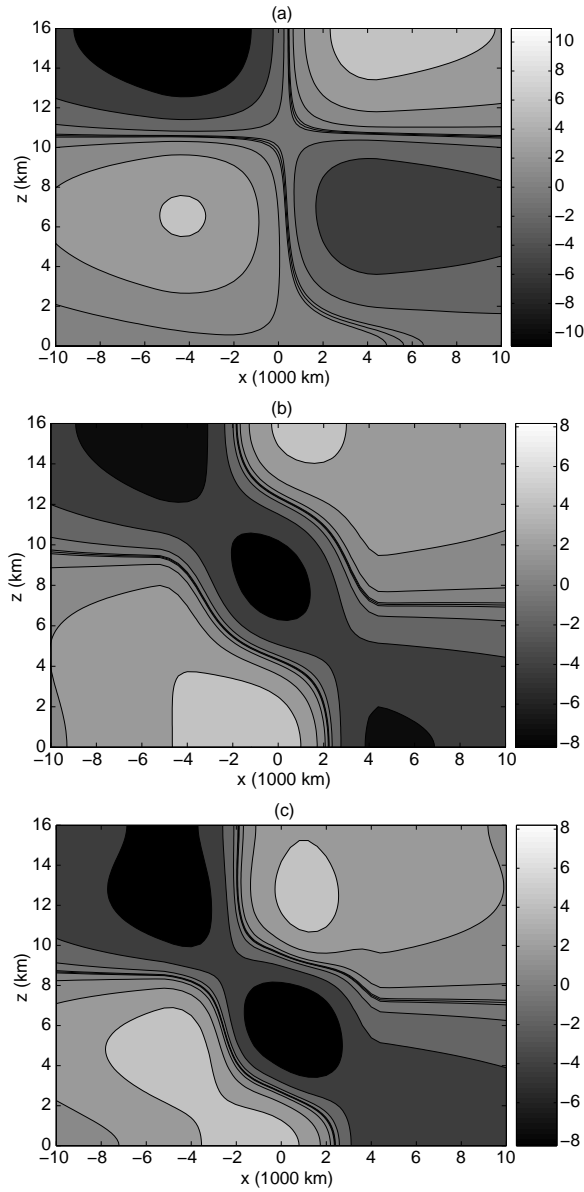


Figure 4: Summary of the kinematic model for the MJO. Contours of zonal velocity u as a function of latitude x and height z , with the leading edge of the MJO shown to the right of the domain. Strongest westerlies (easterlies) are shown in white (black). (a) Upright heating case. (b) Congestus-deep-stratiform tilted heating case. (c) Congestus-deep-stratiform tilted heating case plus effect of upscale momentum transports from synoptic scales. Adapted from Biello and Majda (2005).

velope, one can imagine three scenarios for its physical mechanisms: (i) Does the envelope drive the fluctuations within it? (ii) Do the fluctuations drive the large-scale envelope? (iii) Or do the two evolve cooperatively? This situation is reminiscent of the classic conundrum: Which came first: the chicken or the egg? In atmospheric science, such questions are most familiar from contexts such as midlatitude eddies and jets. Here, instead, the focus is on the tropical case described above, and the evidence will suggest that, in fact, there are cooperative interactions between the envelopes and the fluctuations within them (in addition to those interactions described earlier in the skeleton model).

Before reviewing any results in detail, we review recent and past results on convection–environment interactions. MCS–environment interactions are reviewed first in order to set the stage for the relatively new topic of CCW–environment interactions and in order to highlight their similarities and differences.

MCS–environment interactions have been studied in both “directions,” i.e., the effect of MCS on the environment and vice versa. On the one hand, it is well-known that MCS can have important effects on the larger-scale atmospheric state in which they exist (Houze, 2004). For example, precipitation and vertical transports of temperature and moisture can significantly alter the larger-scale thermodynamic environment. A less-understood effect of MCS on their larger-scale environment is convective momentum transport (CMT). A pervasive aspect of this is the idea of “cumulus friction”; however, many studies have also shown that the CMT of some MCS can actually accelerate the background wind (LeMone and Moncrieff, 1994; Wu and Yanai, 1994; Tung and Yanai, 2002a,b). On the other hand, these interactions also proceed in the opposite direction: the background state – including the wind shear and moist thermodynamic state – affects the MCS that form within it. The environmental thermodynamic state helps determine the intensity of MCS, and the vertical wind shear $\partial u/\partial z$ helps determine their propagation direction and morphology (Barnes and Sieckman, 1984; LeMone et al., 1998; Liu and Moncrieff, 2001).

On larger scales than MCS are the synoptic-scale phenomena known as CCW (Kiladis et al., 2009). With typical wavelengths of 2,000–8,000 km and periods of 2–10 days, CCW are the dominant synoptic-scale weather features in many regions in the tropics, but they are less understood than the smaller-scale MCS. Just as MCS interact with their larger-scale environment, so do CCW. However, CCW–environment interactions are in a relatively primitive stage of understanding.

On the one hand, one might suspect that CCW can affect their larger-scale environment as MCS do. Some results using diagnostic models for the CCW have demonstrated that this is true [see Haertel and Kiladis (2004), Biello et al. (2007), and references therein]. For example, CCW can act as heat sources and moisture sinks for their environment, as was represented by the $\bar{H}a$ terms of the MJO skeleton model in (1). Also, since they have tilts in the vertical/zonal direction (Takayabu et al., 1996; Straub and Kiladis, 2003), CCW circulations can transport momentum to larger scales. That is to say, eddy flux divergences can accelerate or decelerate the mean flow, where the CCW are the “eddies”

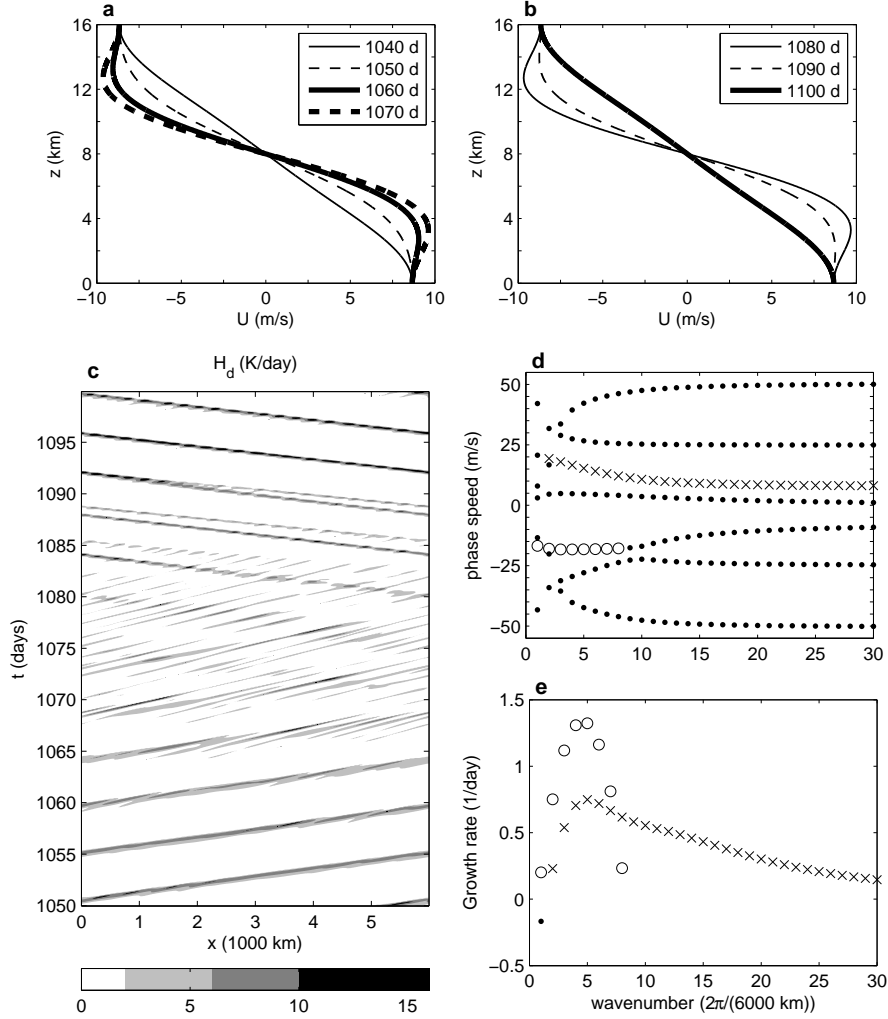


Figure 5: Summary of the dynamic model for waves in the MJO, with a demonstration of CCW–mean flow interactions on intraseasonal time scales. Snapshots of mean wind $\bar{U}(z, t)$ from (a) times $t = 1040$ – 1070 days, and (b) times $t = 1080$ – 1100 days. (c) Contours of deep convective heating $H_d(x, t)$ as a function of latitude x and time t . (d) Phase speeds of linear waves with a background shear given by the mean wind at time $t = 1080$ days. (e) Growth rates of the linear waves in this background shear. Unstable modes are plotted with ‘x’ and ‘o’ for the westward- and eastward-propagating modes, respectively. Adapted from Majda and Stechmann (2009b).

in this context. This has important implications for the MJO, as shown in the kinematic multi-scale models of Biello and Majda (2005) and Biello et al. (2007). As illustrated here in Figure 4, they show that the westerly jet of the MJO’s westerly wind burst can be driven by momentum transports from synoptic-scale CCW.

On the other hand, one might also suspect CCW–environment interactions to occur in the other direction; i.e., one might suspect that the background state – including the background wind and moist thermodynamic state – can affect the CCW that form within it. Unfortunately, while several studies have documented the properties of CCW, few have documented them in different, distinct background environments [exceptions to this include Roundy and Frank (2004) and Yang et al. (2007)]. Besides observations, computer simulations of CCW have presently offered little insight into CCW–environment interactions, since GCMs do not adequately capture CCW (Lin et al., 2006), and simulations of CCW with cloud-resolving models (CRMs) are challenging [but not impossible: see Grabowski and Moncrieff (2001), Tulich et al. (2007), and discussion below]. One promising method for numerical simulations of CCW is the so-called “multi-cloud model” in recent work of Khouider and Majda (2006, 2007, 2008a,b), which has been successful in capturing observed features of CCW and in explaining their physical mechanisms. Building on earlier work, the multi-cloud model includes parameterization of three cloud types – congestus, stratiform, and deep convective clouds – and their different vertical structures: a deep convective heating mode and a second vertical mode with low-level heating and cooling corresponding to congestus and stratiform clouds. Detailed linear stability analysis and nonlinear simulations reveal a mechanism for large-scale instability of moist gravity waves. The model reproduces key features of the observational record for CCW (Kiladis et al., 2009), including their phase speeds and their horizontal and vertical structures.

Since the multi-cloud model of Khouider and Majda (2006, 2007, 2008a,b) captures realistic CCW, it can be used for studies of CCW–environment interactions. This has been done by Majda and Stechmann (2009b), who designed a multi-scale framework for interactions of CCW and background wind shear, i.e., convectively coupled wave–mean flow interactions. The mean flow can affect the CCW through advection, and the CCW can drive changes in the mean flow through CMT. Conceptually, the model then takes the form (using the zonal velocity as an example)

$$\frac{\partial \bar{U}}{\partial T} + \frac{\partial}{\partial z} \overline{w'u'} = 0 \quad (5)$$

$$\frac{\partial u'}{\partial t} + \bar{U} \frac{\partial u'}{\partial x} + w' \frac{\partial \bar{U}}{\partial z} + \frac{\partial p'}{\partial x} = S'_{u,1} \quad (6)$$

where \bar{U} is the large-scale mean wind and u' represents the synoptic-scale waves. In mathematical form, the key interactions are (i) eddy flux convergence of wave momentum $\partial_z \overline{w'u'}$ driving changes in the mean flow \bar{U} , and (ii) advection of the waves u' by the mean flow \bar{U} . Also note that the time scale $T = \epsilon^2 t$ for the

changes of the zonal mean flows in (5) is longer than that for the waves, i.e., intraseasonal rather than synoptic; this arises as part of a multi-scale asymptotic derivation in Majda and Stechmann (2009b). While only the large-scale mean wind \bar{U} is displayed in (5)–(6), the large-scale mean water vapor \bar{Q} and potential temperature $\bar{\Theta}$ were also part of the model in Majda and Stechmann (2009b), but they had little effect (perhaps because there is no large-scale moisture convergence in this setup).

Results from the CCW–mean flow model (5)–(6) are shown in Figure 5 [see Majda and Stechmann (2009b) for further results]. This figure shows the evolution of the CCW–mean flow system through one cycle of its evolution, which proceeds on an intraseasonal time scale. Figures 5a and 5b show the evolution of the mean wind, $\bar{U}(z, t)$, and Figure 5c shows the simultaneous evolution of the CCWs. Initially, at time $t = 1050$ days, an eastward-propagating CCW is favored in a background shear that resembles the westerly onset phase of the MJO, with strongest westerlies at the surface. As time progresses, the CMT from this CCW accelerates the strongest westerlies aloft by time $t = 1070$ days, as in the westerly wind burst phase of the MJO (Lin and Johnson, 1996). In this way, the CCW essentially creates its own demise, since the eastward-propagating wave is unfavorable in the presence of this low-level westerly jet, as shown in Figure 5c as it weakens, breaks up, and reforms as a westward-propagating wave from times $t = 1065$ –1085 days. This westward-propagating wave, in turn, then decelerates the mean wind from $t = 1085$ –1100 days, and the cycle continues, thereby demonstrating that momentum transports from CCW can sometimes accelerate and sometimes decelerate the mean wind. The favorability of the eastward- or westward-propagating wave in a given wind shear can be corroborated by linear theory, an example of which is shown in Figures 5d and 5e for the jet shear at time $t = 1080$. At this time, the westward-propagating wave has the largest growth rates on the large scales, but the eastward-propagating waves have significant nonzero growth rates on smaller scales; this leads to the multi-scale wave structure at this time in Figure 5c, where the CCW appears as a westward-propagating envelope of smaller-scale, eastward-propagating features that resemble squall lines. In summary, this model demonstrates CCW–mean flow interactions in a dynamical setting: the mean wind determines the preferred propagation direction of the CCW, and, simultaneously, CMT from the CCW can sometimes accelerate and sometimes decelerate the mean wind, all on an intraseasonal time scale.

4 Implications for GCMs

Given the wide range of interactions in the hierarchy of organized tropical convection, it is maybe not surprising that GCMs struggle with capturing CCW and the MJO (Moncrieff and Klinker, 1997; Lin et al., 2006). With grid spacings of roughly 100 km, GCMs can at best hope to capture convection on scales of roughly 1000 km and larger (i.e., CCW and the MJO), assuming about 10 grid points are needed to properly resolve a given feature. This also implies

that features with scales of 100-1000 km and smaller must be parameterized; MCS fall within this category but are often ignored in parameterizations. These two problems – properly representing CCW and properly parameterizing MCS – are crucial to improving the MJO and the hierarchy of organized convection in GCMs (Moncrieff et al., 2007).

A convective parameterization that captures realistic CCW is the multi-cloud parameterization of Khouider and Majda (2006, 2007, 2008a,b), which includes several features that are not standard among contemporary convective parameterizations. The key aspect of this parameterization is the representation of three different cloud types: congestus, deep convection, and stratiform clouds (Johnson et al., 1999; Houze, 2004). Each of these different phases of convection plays a different role in the heat and moisture budgets, and it is important to include all three phases rather than just deep convection (Haertel and Kiladis, 2004; Khouider and Majda, 2006, 2008b). The congestus phase of convection appears to be important for moistening the lower troposphere during the MJO’s suppressed stage (Kikuchi and Takayabu, 2004; Tian et al., 2006). However, GCMs do not appear to properly represent congestus clouds and the accompanying moistening effects. It is possible that parameterizations with minimum entrainment parameters, which have improved the strength of intraseasonal variability in some GCMs, are employing a surrogate for congestus clouds and lower tropospheric moistening (Tokioka et al., 1988; Sobel et al., 2009). In addition, the direct effect of the stratiform phase of convection is present in the multi-cloud models but largely absent in contemporary GCMs, yet it is important due to the unsaturated downdrafts in the stratiform region, which can cool and dry the lower troposphere and boundary layer and generate cold pools (Mapes, 2000).

While the earliest studies with the multi-cloud model used a simplified dynamical core, the multi-cloud model convective parameterization was recently coupled to NCAR’s next-generation dry dynamical core GCM (Khouider et al., 2010). With a coarse GCM resolution of 167 km in an aquaplanet setup, the multi-cloud parameterization succeeds in reproducing a realistic MJO with all of the features I–III and also dynamically consistent with the skeleton model (Majda and Stechmann, 2009a) described earlier. This model parameterization also produces realistic convectively coupled equatorial waves (Kiladis et al., 2009; Khouider et al., 2010). Furthermore, the computational overhead of the multi-cloud convective parameterization is less than 1% of the dry dynamical core. In comparison, features of the MJO are also captured by the superparameterization techniques pioneered by Grabowski (2001, 2004), and these techniques have recently improved the quality of MJO’s beyond coarse GCM parameterization in realistic climate models (Khairoutdinov et al., 2008; Benedict and Randall, 2009); of course, the computational overhead in such superparameterization algorithms is substantial beyond the dry dynamical core. An active area of research is the search for cheaper versions of superparameterization that retain statistical fidelity of the multi-scale interactions (Jung and Arakawa, 2005; Grabowski, 2006; Xing et al., 2009).

In addition to moist thermodynamic effects, unresolved MCS can also af-

fect resolved GCM dynamics in other ways. One way is convective momentum transport (CMT). It has been recognized that CMT can either accelerate or decelerate the mean wind (LeMone and Moncrieff, 1994; Wu and Yanai, 1994), and representations of this feature have been included in parameterizations that have improved climatological-scale circulations (Wu et al., 2007; Richter and Rasch, 2008). However, observations also show that the acceleration/deceleration due to CMT occurs in intense, intermittent bursts (Tung and Yanai, 2002a,b), and including this intermittency should be important for the variability of resolved convection. A promising method for including the intermittent aspects of unresolved CMT is the stochastic parameterization of Majda and Stechmann (2008), which should help increase the variability of CCW and the MJO, which tends to be significantly lower in GCMs than in observations (Lin et al., 2006).

It is possible that lessons for GCMs can be learned from CRM simulations of multi-scale convection, since CRMs are able to represent a CCW envelope and the MCS within it, whereas GCMs struggle to capture the MJO envelope and the CCW within it. For instance, the role of CMT and momentum damping can be seen in CRM simulations of CCW. One subtle aspect of these CRM simulations is that the role of *resolved* momentum transports appears to depend on the strength of *parameterized* momentum damping. The simulations of Grabowski and Moncrieff (2001) employ (parameterized) weak momentum damping with a time scale of 24 hours, and the results show that resolved CMT from MCS plays an important role in driving the CCW envelope. On the other hand, the simulations of Tulich et al. (2007) employ (parameterized) stronger momentum damping with a time scale of 4 hours, and they find little role of resolved CMT in driving the CCW envelope; instead, the key mechanism involves interactions between MCS and gravity waves generated by the MCS (Mapes, 1993; Tulich and Mapes, 2008; Stechmann and Majda, 2009). Other CRM simulations of Held et al. (1993) show two extreme cases with (i) no CMT allowed and (ii) no momentum damping, and the results are completely different in the two cases. Given this variety of results, it is likely that parameterized CMT in GCMs strongly affects the resolved waves – i.e., CCW and the MJO – and the simulated mechanisms behind them.

5 Summary

Observations show that the MJO is an envelope of smaller-scale convective processes. Based on these observations, several multi-scale theories and models for the MJO have been developed recently, and they were reviewed here.

A simple model for the MJO skeleton predicts its fundamental features I–III on planetary/intraseasonal scales (section 2), including a simple formula for the MJO’s frequency:

$$\omega \approx \sqrt{\Gamma \bar{R}(1 - \tilde{Q})}. \quad (7)$$

The fundamental mechanism for the MJO in this model involves neutrally stable interactions between (i) planetary-scale, lower-tropospheric moisture anomalies

and (ii) synoptic-scale, convectively-coupled-wave activity.

Many of the MJO's more refined features are captured by additional multi-cloud and multi-scale effects (section 3). Basic multi-cloud effects recover the tilted zonal-vertical structure of the MJO, as shown in a kinematic multi-scale model. This model also demonstrates how the westerly wind burst can intensify aloft due to upscale momentum fluxes from synoptic-scale CCWs. Basic multi-scale effects were further demonstrated with a dynamic multi-scale model for interactions between CCW and a mean wind shear. This model also reproduces westerly wind burst intensification aloft, as did the kinematic model, but it does so in a dynamic setting where the waves can also respond to changes in the mean wind – i.e., a dynamical setting of CCW–mean flow interaction.

Finally, based on the success of these multi-scale models and theories in explaining features of the MJO, it was suggested that the key to simulating the MJO in GCMs is to properly represent the hierarchy of organized convection across all scales (section 4). Ultimately, this means that GCMs must properly capture CCWs, which will require a proper parameterization of unresolved convection on mesoscales and smaller scales. Two key aspects of this are the parameterization of multiple cloud types – congestus, deep convection, and stratiform – and convective momentum transport. While some of these have long been challenging issues, recent results have suggested new ideas and shown further progress.

References

- Barnes, G. and K. Sieckman, 1984: The environment of fast-and slow-moving tropical mesoscale convective cloud lines. *Monthly Weather Review*, **112** (9), 1782–1794.
- Benedict, J. and D. Randall, 2009: Structure of the Madden-Julian Oscillation in the Superparameterized CAM. *J. Atmos. Sci.*, **66** (11), 3277–3296.
- Biello, J. A. and A. J. Majda, 2005: A new multiscale model for the Madden-Julian oscillation. *J. Atmos. Sci.*, **62**, 1694–1721.
- Biello, J. A. and A. J. Majda, 2006: Modulating synoptic scale convective activity and boundary layer dissipation in the IPESD models of the Madden-Julian oscillation. *Dyn. Atmos. Oceans*, **42**, 152–215.
- Biello, J. A., A. J. Majda, and M. W. Moncrieff, 2007: Meridional momentum flux and superrotation in the multi-scale IPESD MJO model. *J. Atmos. Sci.*, **64** (5), 1636–1651.
- Caballero, R. and M. Huber, 2010: Spontaneous transition to superrotation in warm climates simulated by CAM3. *Geophys. Res. Lett.*, **37** (11), L11 701.
- Chao, W. C., 1987: On the origin of the tropical intraseasonal oscillation. *J. Atmos. Sci.*, **44**, 1940–1949.
- Gill, A., 1980: Some simple solutions for heat-induced tropical circulation. *Q. J. Royal Meteor. Soc.*, **106** (449), 447–462.
- Grabowski, W. W., 2001: Coupling cloud processes with the large-scale dynamics using the cloud-resolving convection parameterization (CRCP). *J. Atmos. Sci.*, **58**, 978–997.

- Grabowski, W. W., 2003: MJO-like coherent structures: sensitivity simulations using the cloud-resolving convection parameterization (CRCP). *J. Atmos. Sci.*, **60**, 847–864.
- Grabowski, W. W., 2004: An improved framework for superparameterization. *J. Atmos. Sci.*, **61**, 1940–1952.
- Grabowski, W. W., 2006: Comments on “Preliminary tests of multiscale modeling with a two-dimensional framework: sensitivity to coupling methods”. *Mon. Wea. Rev.*, **134**, 2021–2026.
- Grabowski, W. W. and M. W. Moncrieff, 2001: Large-scale organization of tropical convection in two-dimensional explicit numerical simulations. *Q. J. Roy. Met. Soc.*, **127**, 445–468.
- Grabowski, W. W. and M. W. Moncrieff, 2004: Moisture-convection feedback in the Tropics. *Q. J. Roy. Met. Soc.*, **130**, 3081–3104.
- Haertel, P. T. and G. N. Kiladis, 2004: Dynamics of 2-day equatorial waves. *J. Atmos. Sci.*, **61**, 2707–2721.
- Held, I., R. Hemler, and V. Ramaswamy, 1993: Radiative-convective equilibrium with explicit two-dimensional moist convection. *J. Atmos. Sci.*, **50** (23), 3909–3927.
- Hendon, H. H. and B. Liebmann, 1994: Organization of convection within the Madden–Julian oscillation. *J. Geophys. Res.*, **99**, 8073–8084, doi:10.1029/94JD00045.
- Hendon, H. H. and M. L. Salby, 1994: The life cycle of the Madden–Julian oscillation. *J. Atmos. Sci.*, **51**, 2225–2237.
- Houze, R. A., 2004: Mesoscale convective systems. *Rev. Geophys.*, **42**, G4003+, doi:10.1029/2004RG000150.
- Houze, R. A., Jr., S. S. Chen, D. E. Kingsmill, Y. Serra, and S. E. Yuter, 2000: Convection over the Pacific warm pool in relation to the atmospheric Kelvin–Rossby wave. *J. Atmos. Sci.*, **57**, 3058–3089.
- Johnson, R. H., T. M. Rickenbach, S. A. Rutledge, P. E. Ciesielski, and W. H. Schubert, 1999: Trimodal characteristics of tropical convection. *J. Climate*, **12**, 2397–2418.
- Jung, J.-H. and A. Arakawa, 2005: Preliminary tests of multiscale modeling with a two-dimensional framework: sensitivity to coupling methods. *Mon. Wea. Rev.*, **133** (3), 649–662.
- Khairoutdinov, M., C. DeMott, and D. Randall, 2008: Evaluation of the simulated interannual and subseasonal variability in an AMIP-style simulation using the CSU Multiscale Modeling Framework. *J. Climate*, **21** (3), 413–431.
- Khouider, B. and A. J. Majda, 2006: A simple multicloud parameterization for convectively coupled tropical waves. Part I: Linear analysis. *J. Atmos. Sci.*, **63**, 1308–1323.
- Khouider, B. and A. J. Majda, 2007: A simple multicloud parameterization for convectively coupled tropical waves. Part II: Nonlinear simulations. *J. Atmos. Sci.*, **64**, 381–400.
- Khouider, B. and A. J. Majda, 2008a: Equatorial convectively coupled waves in a simple multicloud model. *J. Atmos. Sci.*, **65**, 3376–3397.
- Khouider, B. and A. J. Majda, 2008b: Multicloud models for organized tropical convection: enhanced congestus heating. *J. Atmos. Sci.*, **65**, 895–914.

- Khouider, B., A. St-Cyr, A. J. Majda, and J. Tribbia, 2010: MJO and convectively coupled waves in a coarse resolution GCM with a simple multcloud parameterization. *J. Atmos. Sci.*, submitted.
- Kikuchi, K. and Y. N. Takayabu, 2004: The development of organized convection associated with the MJO during TOGA COARE IOP: Trimodal characteristics. *Geophys. Res. Lett.*, **31** (10.1029).
- Kiladis, G. N., K. H. Straub, and P. T. Haertel, 2005: Zonal and vertical structure of the Madden–Julian oscillation. *J. Atmos. Sci.*, **62**, 2790–2809.
- Kiladis, G. N., M. C. Wheeler, P. T. Haertel, K. H. Straub, and P. E. Roundy, 2009: Convectively coupled equatorial waves. *Rev. Geophys.*, **47**, RG2003, doi:10.1029/2008RG000266.
- Lau, W. K. M. and D. E. Waliser, (Eds.) , 2005: *Intraseasonal Variability in the Atmosphere–Ocean Climate System*. Springer, Berlin.
- LeMone, M. and M. Moncrieff, 1994: Momentum and mass transport by convective bands: comparisons of highly idealized dynamical models to observations. *J. Atmos. Sci.*, **51** (2), 281–305.
- LeMone, M., E. Zipser, and S. Trier, 1998: The role of environmental shear and thermodynamic conditions in determining the structure and evolution of mesoscale convective systems during TOGA COARE. *J. Atmos. Sci.*, **55** (23), 3493–3518.
- Lin, J.-L., et al., 2006: Tropical intraseasonal variability in 14 IPCC AR4 climate models Part I: Convective signals. *J. Climate*, **19**, 2665–2690.
- Lin, X. and R. H. Johnson, 1996: Kinematic and thermodynamic characteristics of the flow over the western Pacific warm pool during TOGA COARE. *J. Atmos. Sci.*, **53**, 695–715.
- Liu, C. and M. Moncrieff, 2001: Cumulus ensembles in shear: implications for parameterization. *J. Atmos. Sci.*, **58** (18), 2832–2842.
- Majda, A. J., 2003: *Introduction to PDEs and Waves for the Atmosphere and Ocean*, Courant Lecture Notes in Mathematics, Vol. 9. American Mathematical Society, Providence, x+234 pp.
- Majda, A. J. and J. A. Biello, 2004: A multiscale model for the intraseasonal oscillation. *Proc. Natl. Acad. Sci. USA*, **101** (14), 4736–4741.
- Majda, A. J. and R. Klein, 2003: Systematic multiscale models for the Tropics. *J. Atmos. Sci.*, **60**, 393–408.
- Majda, A. J. and S. N. Stechmann, 2008: Stochastic models for convective momentum transport. *Proc. Natl. Acad. Sci.*, **105**, 17 614–17 619.
- Majda, A. J. and S. N. Stechmann, 2009a: The skeleton of tropical intraseasonal oscillations. *Proc. Natl. Acad. Sci.*, **106** (21), 8417.
- Majda, A. J. and S. N. Stechmann, 2009b: A simple dynamical model with features of convective momentum transport. *J. Atmos. Sci.*, **66**, 373–392.
- Majda, A. J., S. N. Stechmann, and B. Khouider, 2007: Madden–Julian Oscillation analog and intraseasonal variability in a multcloud model above the equator. *Proc. Natl. Acad. Sci. USA*, **104** (24), 9919–9924.
- Mapes, B., 1993: Gregarious tropical convection. *J. Atmos. Sci.*, **50** (13), 2026–2037.

- Mapes, B. E., 2000: Convective inhibition, subgrid-scale triggering energy, and stratiform instability in a toy tropical wave model. *J. Atmos. Sci.*, **57**, 1515–1535.
- Masunaga, H., T. L’Ecuyer, and C. Kummerow, 2006: The Madden–Julian oscillation recorded in early observations from the Tropical Rainfall Measuring Mission (TRMM). *J. Atmos. Sci.*, **63** (11), 2777–2794.
- Matsuno, T., 1966: Quasi-geostrophic motions in the equatorial area. *J. Meteor. Soc. Japan*, **44** (1), 25–43.
- Moncrieff, M. W., 2004: Analytic representation of the large-scale organization of tropical convection. *J. Atmos. Sci.*, **61**, 1521–1538.
- Moncrieff, M. W. and E. Klinker, 1997: Organized convective systems in the tropical western Pacific as a process in general circulation models: a TOGA COARE case-study. *Q. J. Roy. Met. Soc.*, **123** (540), 805–827.
- Moncrieff, M. W., M. Shapiro, J. Slingo, and F. Molteni, 2007: Collaborative research at the intersection of weather and climate. *WMO Bull.*, **56**, 204–211.
- Nakazawa, T., 1988: Tropical super clusters within intraseasonal variations over the western Pacific. *J. Met. Soc. Japan*, **66** (6), 823–839.
- Richter, J. and P. Rasch, 2008: Effects of convective momentum transport on the atmospheric circulation in the Community Atmosphere Model, Version 3. *J. Climate*, **21** (7), 1487–1499.
- Roundy, P. and W. Frank, 2004: A climatology of waves in the equatorial region. *J. Atmos. Sci.*, **61** (17), 2105–2132.
- Salby, M. and H. Hendon, 1994: Intraseasonal behavior of clouds, temperature, and motion in the tropics. *J. Atmos. Sci.*, **51** (15), 2207–2224.
- Sobel, A. H., E. D. Maloney, G. Bellon, and D. M. Frierson, 2009: Surface fluxes and tropical intraseasonal variability: a reassessment. *J. Adv. Model. Earth Syst.*, in press.
- Stechmann, S. N. and A. J. Majda, 2009: Gravity waves in shear and implications for organized convection. *J. Atmos. Sci.*, **66**, 2579–2599.
- Straub, K. H. and G. N. Kiladis, 2003: The observed structure of convectively coupled Kelvin waves: comparison with simple models of coupled wave instability. *J. Atmos. Sci.*, **60** (14), 1655–1668.
- Takayabu, Y. N., K. M. Lau, and C. H. Sui, 1996: Observation of a quasi-2-day wave during TOGA COARE. *Monthly Weather Review*, **124** (9), 1892–1913.
- Tian, B., D. Waliser, E. Fetzer, B. Lambrechtsen, Y. Yung, and B. Wang, 2006: Vertical moist thermodynamic structure and spatial-temporal evolution of the MJO in AIRS observations. *J. Atmos. Sci.*, **63** (10), 2462–2485.
- Tokioka, T., K. Yamazaki, A. Kitoh, and T. Ose, 1988: The equatorial 30–60 day oscillation and the Arakawa–Schubert penetrative cumulus parameterization. *Journal of the Meteorological Society of Japan*, **66** (6), 883–901.
- Tulich, S. and B. Mapes, 2008: Multi-scale convective wave disturbances in the Tropics: Insights from a two-dimensional cloud-resolving model. *J. Atmos. Sci.*, **65** (1), 140–155.
- Tulich, S. N., D. Randall, and B. Mapes, 2007: Vertical-mode and cloud decomposition of large-scale convectively coupled gravity waves in a two-dimensional cloud-resolving model. *J. Atmos. Sci.*, **64**, 1210–1229.

- Tung, W. and M. Yanai, 2002a: Convective momentum transport observed during the TOGA COARE IOP. Part I: General features. *J. Atmos. Sci.*, **59** (11), 1857–1871.
- Tung, W. and M. Yanai, 2002b: Convective momentum transport observed during the TOGA COARE IOP. Part II: Case studies. *J. Atmos. Sci.*, **59** (17), 2535–2549.
- Wang, B., 2005: Theory. *Intraseasonal Variability in the Atmosphere–Ocean Climate System*, W. K. M. Lau and D. E. Waliser, Eds., Springer, Berlin.
- Wheeler, M. and G. N. Kiladis, 1999: Convectively coupled equatorial waves: analysis of clouds and temperature in the wavenumber–frequency domain. *J. Atmos. Sci.*, **56** (3), 374–399.
- Wu, X., L. Deng, X. Song, and G. Zhang, 2007: Coupling of convective momentum transport with convective heating in global climate simulations. *J. Atmos. Sci.*, **64** (4), 1334–1349.
- Wu, X. and M. Yanai, 1994: Effects of vertical wind shear on the cumulus transport of momentum: observations and parameterization. *J. Atmos. Sci.*, **51** (12), 1640–1660.
- Xing, Y., A. J. Majda, and W. W. Grabowski, 2009: New efficient sparse space-time algorithms for superparameterization on mesoscales. *Monthly Weather Review*, **137**, 4307–4324.
- Yanai, M., B. Chen, and W.-W. Tung, 2000: The Madden–Julian oscillation observed during the TOGA COARE IOP: Global view. *J. Atmos. Sci.*, **57**, 2374–2396.
- Yang, G., B. Hoskins, and J. Slingo, 2007: Convectively coupled equatorial waves. Part I: Horizontal and vertical structures. *J. Atmos. Sci.*, **64** (10), 3406–3423.
- Zhang, C., 2005: Madden–Julian Oscillation. *Reviews of Geophysics*, **43**, G2003+, doi:10.1029/2004RG000158.